

IRREGULAR CONDITIONS OF OBLIQUE COLLISION OF SHOCK WAVES IN SOLID BODIES

L. V. AL'TSHULER, S. B. KORMER, A. A. BAKANOVA, A. P. PETRUNIN, A. I. FUNTIKOV, and A. A. GUBKIN

Submitted to JETP editor May 18, 1961

J. Exptl. Theoret. Phys. (U.S.S.R.) 41, 1382-1393 (November, 1961)

A method for producing and recording irregular modes of shock-wave collisions in solids is described. The parameters of three-shock configurations due to the collision of 300-400 thousand atm and 1.0-1.8 million atm shock waves are presented for four metals. In the first series of experiments a six- to eightfold pressure increase was observed at angles close to the critical angles of appearance of the leading waves. For waves of greater amplitude the pressure increased to 4 million atm for aluminum and to 7 million atm for steel, copper, and lead in the collision region when the waves cross at right angles.

The results obtained are analyzed by the method of shock-wave polar curves. It is shown that the model with a single tangential discontinuity cannot describe irregular modes of oblique collision of "weak" shock waves in metals. A method is described for determining the pressure and density behind the reflected wave front from the parameters of the three-shock configurations. As an example, the pressures and densities are calculated for the collision of strong shock waves in aluminum. Consecutive compression by the incident and reflected waves increased the density of aluminum by 2.26 times, i.e., to 6.12 g/cm³.

INTRODUCTION

THE transition from regular to irregular reflection is connected with the appearance of a leading wave moving away from the reflecting wall; this wave forms together with the incident and reflected waves a characteristic three-shock configuration (Fig. 1). Irregular reflections of air shock waves were discovered in 1869 by E. Mach. They were subsequently the subject of numerous experimental researches, described in sufficient detail in the review by Bleakney and Taub.^[1]

The theory of a three-shock configuration in a perfect gas has been treated by Landau and Lifshitz^[2] and by Courant and Friedrichs.^[3] The simplest and most probable flow is usually assumed to have a single tangential discontinuity between the region of single compression (behind the front of the leading wave) and the region of the two-stage (or double) compression of the reflected wave. Nonlinear reflections of weak shock waves in air were recently calculated by Ryzhov and Khristyanovich.^[4] The flow modes are characterized in this case by large pressure gradients both along the normal to the discontinuity surface and along the front of the leading wave.

The conditions under which three-shock configuration occurs in certain condensed substances were examined by Zel'dovich and Gandel'man in 1947. At approximately the same time the leading

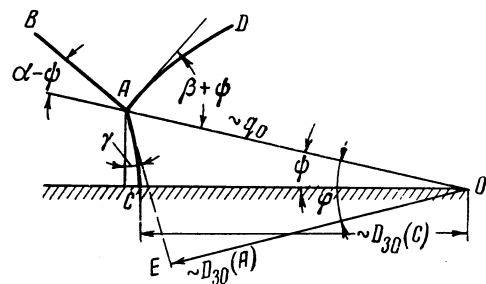


FIG. 1. Diagram of three-shock configuration: AB - incident wave, AD - reflected wave, AC - frontal wave, OA - trajectory of the branching point, OC - mass of frontal wave, proportional to $D_{30}(C)$, OE - segment proportional to $D_{30}(A)$.

wave in solids was observed experimentally by Feoktistova,^[5] who recorded with a high-speed photochronograph pictures of collisions between shock waves in a solid explosive and in aluminum.

We report in this article the results of experimental studies of irregular modes in solids, undertaken by the authors to determine their equations of state. An oblique collision between shock waves results in regions of extra high pressures, several times greater than the pressures of the incoming incident shock waves prior to collision.

Compressibility is of greatest interest in the regions of two-stage compression behind the fronts of reflected waves. The successive application of the pressures of the incoming and reflected waves

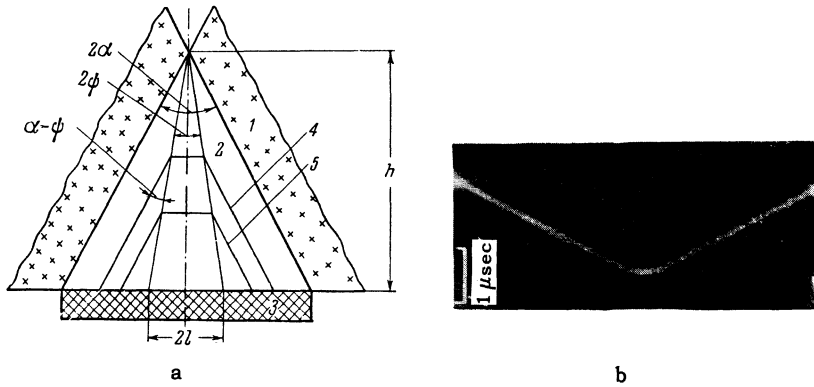


FIG. 2. a - diagram of the first series of experiments. 1 - charge of explosive, 2 - prismatic specimen with vertex angle 2α , 3 - Plexiglas plate, 4, 5 - fronts of three-shock configurations at different instants of time, h - height of specimen, $2l$ - width of leading wave at the instant of emergence to the surface of the Plexiglas; b - photochronogram of three-shock configuration.

results in a smaller increase in the entropy than a single shock transition. The states obtained on the pressure-density diagram in the region of two-fold compression lie therefore below the Hugoniot adiabat and approach essentially the compression curve for absolute zero temperature.

In the first section of this article we describe methods for obtaining and registering three-shock configurations and report the experimental results. We then use several metals of known equations of state as examples to analyze the conditions under which the regular modes set in and the character of the resultant flow. The concluding section considers a method for investigating compressibility by registering the parameters of the irregular reflection.

1. INVESTIGATION PROCEDURE AND EXPERIMENTAL RESULTS

The direct purpose of the experiment was to register the dimensions and the form of the leading wave at a certain fixed distance h from the point of its initiation. The specimens used for the investigation of oblique collision modes were made in the form of isosceles triangular prisms (Fig. 2a). In the first series of experiments plane detonation waves were applied to the side faces of the prisms in synchronism, and produced in the specimens shock waves with amplitudes on the order of several hundred thousand atmospheres. The fronts of the shock waves, parallel to the faces of the specimen, collided at an angle 2α . The angle α ranged from 30 to 60° .

In the second series of experiments pressures on the order of 1 or 2 million atmospheres were obtained by shock in aluminum plates accelerated by the explosion products (Fig. 3a). In this case the investigated specimen with a right-angle vertex was covered with steel plates and was placed in bulky lead blocks with two conical openings. Aluminum pistons were inserted in the openings

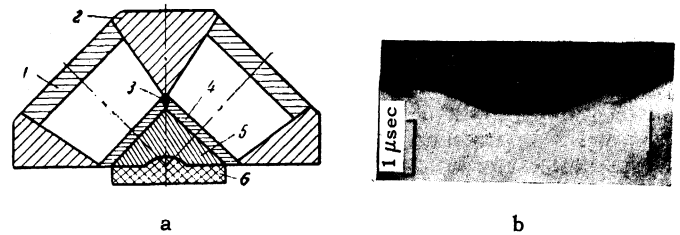


FIG. 3. a - Setup of second series of experiments. 1 - aluminum pistons, 2 - lead blocks, 3 - lead wedge, 4 - steel plates, 5 - specimens, 6 - arched Plexiglas receiver; b - photochronogram obtained with this setup.

of the block from the outside. The explosion products moved the pistons at high speed along the openings, causing them to strike the faces of the specimen in synchronism. The pistons overtook the shock waves in the lead block. A narrow lead wedge inserted between the steel plates guaranteed initiation of the three-shock configuration on the upper edge of the prism.

The specimen heights h were $20-40$ mm in Fig. 2, and $8-14$ mm in Fig. 3. The bases of the specimens were covered with transparent Plexiglas plates.

The collision inside the specimens (Fig. 2a) gave rise to a self-similar propagating configuration with a leading wave located inside a dihedral angle 2ψ . As the incident waves moved on, the line of intersection between the shock fronts and the surface of the Plexiglas shifted gradually from the edges of the specimen to the center of its base. The shift in the front of the wave was accompanied by bright but very brief glow of the air in the gap between the Plexiglas plate and the specimen. The cessation of the glow was due to the dispersion of the Plexiglas by the shock wave. When the leading wave emerged to the lower surface of the specimen, the entire portion of surface ($2l$ wide) occupied by the wave (Fig. 2a) began to glow simultaneously. The consecutive crossings of the transparent plate surface by the waves were

recorded with a high-speed photochronograph through a slit perpendicular to the plane of wave collision. A typical photochronogram is shown in Fig. 2b. The inclined lines of the picture characterize the speed with which the incident wave glides along the base of the specimen, while the tie represents the width of the leading wave at the instant of its emergence to the base of the specimen.

If the gliding speed of the incident waves along the base of the prism is less than the speed of propagation of the shock wave in the Plexiglas, the leading wave may be partially or completely "covered" by the advance waves propagating in the Plexiglas. To avoid this phenomenon, specimens with cylindrical slots in the bases were used (Fig. 3a). When the slot has a cylindrical form, the leading and incident waves emerge to the surface of the convex Plexiglas receiver almost simultaneously. The photochronogram obtained under these conditions is shown in Fig. 3b.

With increasing collision angle α , the dimension of the leading wave increases. Its curvature then becomes noticeable (see the diagram, Fig. 1). The bending is particularly pronounced at large sweep velocities, on the order of several tens of kilometers per second, obtained with the aid of an electron-optical converter. The photochronogram in Fig. 4 of the collision of waves in the aluminum specimen shows quite clearly the bending of the frontal wave. The collision angle 2α was 110° with $\psi = 6^\circ$.

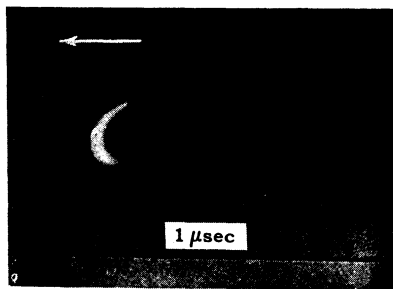


FIG. 4. Photochronogram of three-shock configuration in aluminum, obtained with an electron-optical converter. $P_1 = 0.33 \times 10^{12}$ bar, $\alpha = 55^\circ 20'$, $\psi = 6^\circ$, $h = 86.9$ mm.

In experiments with colliding waves of large amplitude, the bending of the leading wave was registered by placing on the base of the specimen, along a line perpendicular to its axis, a series of contacts shorted by the leading wave as it emerged to the lower surface of the specimen. The successive shorting of the contacts was registered on a high-speed oscilloscope. In estimating the shape of the leading wave and the degree of its bending, the curvature was assumed constant. A quantitative measure of the bending was either the angle γ or $\varphi = \psi + \gamma$ (Fig. 1).

The parameters of the incident shock waves prior to collision were determined in individual experiments by measuring their velocity D_{10} in a direction perpendicular to the side faces of the specimen. The remaining characteristics of the incident waves were determined from the equations of the dynamic adiabats.

Records of the collision process yielded the width $2l$ of the frontal wave and the time difference Δt between the emergences of its edges and of its center from the base of the specimen. Subsequent reduction of the experimental data yielded the angle

$$\psi = \arctg(l/h), \quad (1)^*$$

which the outgoing symmetrical frontal wave makes with the symmetry plane, and the bend angle of the leading wave

$$\gamma = \arctg \frac{2\Delta t D_{10} \cos \psi}{l \sin(\alpha - \psi)}. \quad (2)$$

From these quantities we calculated the velocity of the branching point

$$q_0 = D_{10} / \sin(\alpha - \psi), \quad (3)$$

the velocity and pressure of the leading wave near the branching point

$$D_{30}(A) = q_0 \cos(\psi + \gamma) = q_0 \cos \varphi, \quad (4)$$

$$P_{30}(A) = \rho_0 D_{30}(A) \Delta U_{30}(A), \quad (4a)$$

and the velocity and pressure of the leading wave in the symmetry plane

$$D_{30}(C) = q_0 [\cos \psi - \sin \psi \operatorname{tg}(\gamma/2)], \quad (5)^\dagger$$

$$P_{30}(C) = \rho_0 D_{30}(C) \Delta U_{30}(C). \quad (5a)$$

The discontinuities in the mass velocities $\Delta U_{30}(A)$ and $\Delta U_{30}(C)$ on the front of the leading waves were calculated from the velocities $D_{30}(A)$ and $D_{30}(C)$ by using the equations of the dynamic adiabats. In all the calculations we used the previously determined dynamic single-compression adiabats and the equations of state for lead and copper, [6], iron, [7] and aluminum [6,9].

The parameters of the incoming wave are shown in Table I. The results obtained in the first series of the experiments are plotted as ψ - α and P - α diagrams in Figs. 5a, b, and 6.

The coordinates of Figs. 5a and b are the angle variables ψ and α . Each point is the average of several experiments. All the experiments pertaining to a single material exhibit a rather wide dispersion band. With decreasing α , the slope of the ψ - α curves decreases. This, as well as the dis-

* $\arctg = \tan^{-1}$
 $\dagger \operatorname{tg} = \tan.$

Table I

Metal	First series				Second series			
	D_{10} , km/sec	ΔU_{10} , km/sec	P_1 , 10^{12} bar	σ_1	D_{10} , km/sec	ΔU_{10} , km/sec	P_1 , 10^{12} bar	σ_1
Aluminum	7.48	1.61	0.33	1.27	10.22	3.58	0.99	1.54
Copper	5.15	0.81	0.37	1.19	7.82	2.57	1.79	1.49
Lead	3.33	0.86	0.32	1.33	5.92	2.61	1.75	1.79
Iron	5.38	1.0	0.42	1.23	8.21	2.66	1.71	1.48

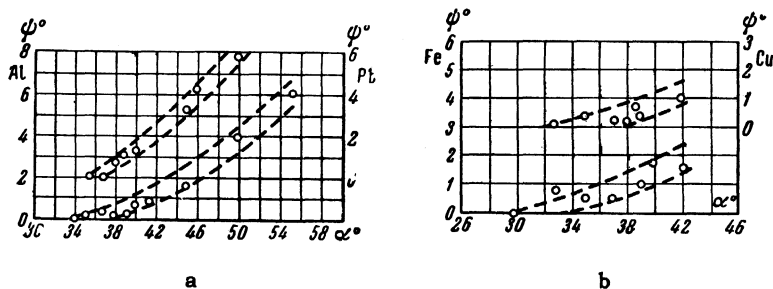


FIG. 5. a - ψ - α diagram of aluminum and lead; b - ψ - α diagram for copper and iron.

persion of the experimental data, does not enable us to determine the accurate values of the critical angles at which irregular modes set in. For aluminum and lead, α_{cr} lies between 34° and 38° and between 35 and 37° ; the ranges are 32° to $37^\circ 30'$ for copper and 30° to 34° for iron.

More detailed data, obtained with aluminum, are found in Table II and in Fig. 6. The left part of Fig. 6 shows the calculated pressures P_2 due to regular reflection. Of the two possible modes, the one with the lower pressures, described by the segment OK, is always realized. There are no solutions for regular reflections at angles $\alpha \geq \alpha_{cr}''$.

The right part of Fig. 6 shows the experimental pressures $P_{30}(C)$ on the symmetry axis, calculated from the data of Table II. When these data were calculated from Eq. (5), the term containing γ was disregarded. When $\alpha - \psi \leq 50^\circ$, the pressure is not overestimated by more than 1 or 2 percent. The bending of the leading wave affects more the pressures near the branching point, calculated by Eq. (4). The resultant values of $P_{30}(A)$ for $\alpha - \psi = 47^\circ 20'$ and $\alpha - \psi = 49^\circ 20'$ are marked in Fig. 6 by points which deviate from the curve $P_{30}(C)$ by 6-8%.

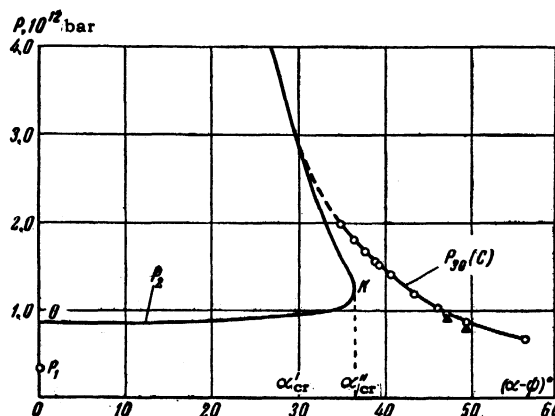


FIG. 6. Pressure of regular and irregular reflections in aluminum. $P_1 = 0.33 \times 10^{12}$ bar.

When $\alpha = 0$, P_2 is a head-on collision pressure which is some 2.5 times greater than the pressure of the incident wave P_1 . The pressure of the leading wave is much higher at collision angles close to the critical angles at which three-shock configuration occurs. Thus, when $\alpha - \psi = 35^\circ$ we have $P_{30}(C) = 2 \times 10^{12}$ bar, which is six times the initial pressure of the colliding waves.

An interesting feature is the appearance of the leading waves at angles $\alpha < \alpha_{cr}''$ in the region

Table II

α	ψ	$P_{30}(C)$, 10^{12} bar	α	ψ	$P_{30}(C)$, 10^{12} bar
34°	0°	—	$41^\circ 40'$	$50'$	1.41
35°	$10'$	1.98	45°	$1^\circ 30'$	1.19
$36^\circ 50'$	$20'$	1.80	50°	$3^\circ 50'$	1.02
$37^\circ 50'$	$10'$	1.87	$55^\circ 20'$	6°	0.86
$39^\circ 10'$	$15'$	1.56	65°	$8^\circ 30'$	0.66
40°	$40'$	1.52			

where regular reflection is still possible. With increasing collision angle the pressures of the leading wave decrease rapidly. Obviously, at gliding-wave angles, i.e., at $\alpha = 90^\circ$, we get $P_{30} = P_1$.

The results of the second series of experiments are listed in Table II. For each metal, the table indicates the pressures of the incident waves, the angles α , ψ , and γ , the propagation velocities of the leading waves near the branch point and on the symmetry plane, and the pressures corresponding to these velocities. The table shows that the wave collision increases the pressure to 4–7 million atmospheres. The angles ψ are accurate to $\pm 30'$. The accuracy in γ is much less.

2. ANALYSIS OF THREE-SHOCK CONFIGURATIONS

In the present section we analyze irregular reflections in copper, aluminum, lead, and iron. We carry out the analysis, following [3], by the method of shock polars in a coordinate system fixed to the branching point A.

In the $U_x - U_y$ diagram (Fig. 7), OO' is the trace of the symmetry plane of the two colliding waves. The plane OO' can be treated also as the boundary surface of an absolutely rigid partition. The trajectory OA of the branching point makes an angle ψ with this surface, and this angle determines the angular aperture of the sector in which the leading wave propagates. In the general case the front of the leading wave is not perpendicular to the surface of the partition, deviating from it by a certain skew angle γ . The half space above the partition is subdivided by the discontinuity surfaces into four regions: rest region — 0, single-shock compression by the incoming shock wave — 1, successive twofold compression by the incoming and reflected waves — 2, single compression by the leading wave — 3.

In the simplest possible flow scheme, regions 2 and 3 are separated from each other by a single surface of tangential discontinuity AT . On both sides of the discontinuity the streams are parallel and the pressures are equal. The fronts of the incoming, reflected, and leading waves make angles $\alpha - \psi$, $\beta + \psi$, and $90^\circ - \varphi$ with the direction OA of propagation of the branching point; $\varphi = \psi + \gamma$.

The vectors ΔU_{10} , ΔU_{21} , and ΔU_{30} in Fig. 7 denote mass-velocity discontinuities on the fronts of the same waves. The stream velocities in region 0, 1, 2, and 3 are given respectively by the vectors q_0 , $q_1 = q_0 + \Delta U_{10}$, $q_2 = q_1 + \Delta U_{21}$, and $q_3 = q_0 + \Delta U_{30}$ (q_3 is not designated in Fig. 7).

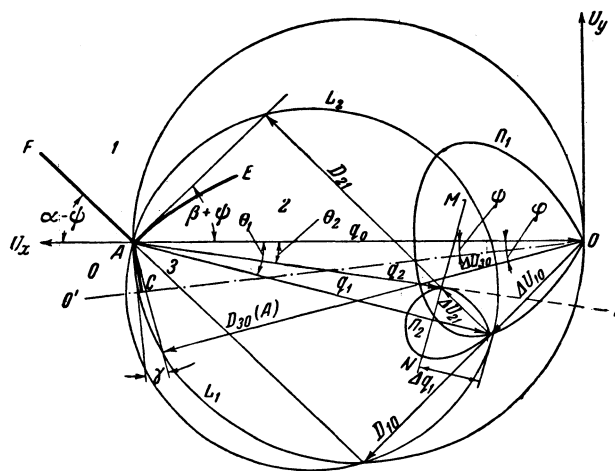


FIG. 7. $U_x - U_y$ diagram of irregular reflection.

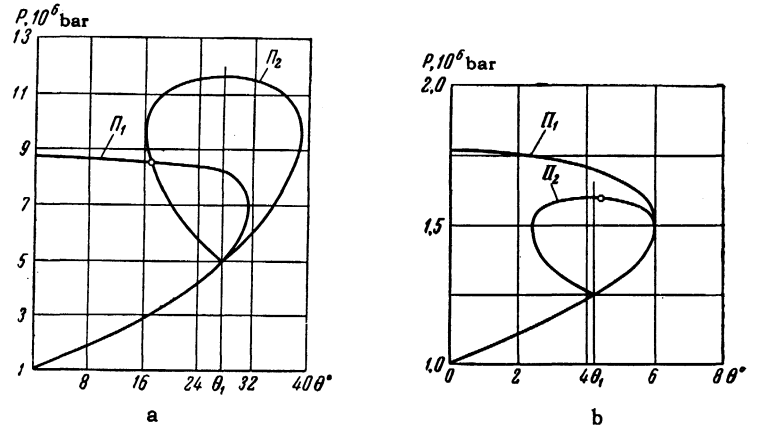
The angle between q_0 and q_1 is θ_1 , while the angles that q_0 makes with q_2 and q_3 are designated θ_2 and θ_3 and are equal to each other. The vectors D_{10} and $D_{30}(A)$ are collinear with ΔU_{10} and ΔU_{30} respectively and are projections of the vector q_0 on the normals to the fronts of the incident and leading waves. The vector D_{21} is an analogous projection of the vector q_1 on the normal to the front of the reflected wave.

Assuming the parameters of the incoming wave, and the vectors q_0 and q_1 (and consequently the angles $\alpha - \psi$ and θ_1) known, we determine the possible states of regions 3 and 2, corresponding to different positions of the discontinuity surfaces of the leading wave and the reflected wave. As the angle φ is varied, the end of the vector D_{30} traces a circular segment L_1 with q_0 as diameter. At the same time the end of the vector ΔU_{30} , which is collinear with D_{30} , traces the shock polar Π_1 . Analogously, as the position of the front AE changes, the end of the vector ΔU_{21} traces the polar Π_2 which is symmetrical relative to the vector q_1 .

The form of the polars is determined by the equations $\Delta U_{30} = f(D_{30})$ and $\Delta U_{21} = f(D_{21})$ of the single and twofold compression adiabats. To each direction of the vector ΔU_{30} corresponds its own angle θ_3 and its pressure $P_{30} = \rho_0 D_{30} \Delta U_{30}$. The analogous quantities for the reflected waves are the angle θ_2 and the pressure $P_2 = P_1 + \rho_1 D_{12} \Delta U_{12}$. Plotted in P and θ coordinates, the relationships between P_3 , θ_3 and P_2 , θ_2 are represented by the curves Π_1 and Π_2 , which are also called shock polars.

By way of an example, Fig. 8a shows the polars of air. When $\theta = 0$ the polar Π_1 crosses the ordinate axis. The maximum pressures at its vertex correspond to shock-wave propagation veloci-

FIG. 8. a—P- θ diagram of oblique collision of “strong” shock waves in air, b—P- θ diagram of oblique collision of “weak” shock waves in air, o—state behind the front of the reflected wave.



ties $D_{30} = q_0$. When the stream deflection angle is $\theta = \theta_1$, the polar Π_1 passes through the incident-wave state. The vertical $\theta = \theta_1$ is the symmetry axis of the polar Π_2 of the reflected wave. Flow with one tangential discontinuity is characterized on the P- θ diagram by the intersection of the polars. Such an intersection, however, does not always take place. In particular, it does not occur, as shown in Fig. 8b, for collisions between “weak” shock waves in air.

Let us turn now to the region of critical angles where the reflection mode turns from regular to irregular. At a certain angle α'_{CR} the polars on the P- θ diagram of Fig. 9a intersect on the ordinate axis. Starting with this instant, irregular reflection can exist for angles $\alpha > \alpha'_{CR}$. Another characteristic angle is $\alpha''_{CR} > \alpha'_{CR}$, at which the polar Π_2 is tangent to the ordinate axes of the P- θ diagram of Fig. 9 and to the symmetry plane on the $U_x - U_y$ diagram of Fig. 7. When $\alpha > \alpha''_{CR}$ the regular mode has no solutions. In the angle interval $\alpha''_{CR} > \alpha > \alpha'_{CR}$ both regular and irregular reflections are possible.

Figure 10 shows the calculated dependence of the critical angles α''_{CR} on the pressures for aluminum, iron, copper, and lead. As $P \rightarrow 0$, $\alpha''_{CR} \rightarrow 90^\circ$. When $P > 50 \times 10^{10}$ bar, the critical angles assume stable values in the range $32^\circ - 38^\circ$. A comparison of the calculated and experimental values (Fig. 5) shows that in aluminum, copper, and possibly also iron the three-shock configuration occurs when $\alpha < \alpha''_{CR}$. In aluminum and copper the difference is $2-3^\circ$. At the same time, the experimental value is $\alpha_{CR} > \alpha'_{CR}$ (see Fig. 6). A possible reason for the occurrence of the leading wave is the transition of the branching point to subsonic motion, at which $c_2 + q_2 > q_0$. For lead the experimental value is $\alpha_{CR} > \alpha''_{CR}$. We attribute this fact to the known experimental error in the determination of the leading wave in the lead specimens, the reason for which was explained in the preceding section.

FIG. 9. P- θ diagrams at critical collision angles.

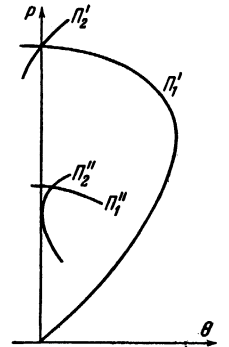


FIG. 10. Dependence of the critical angles α'' of aluminum, copper, lead, and iron on the pressure of the colliding waves.

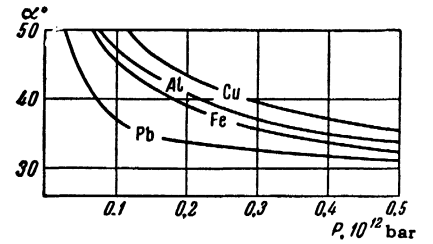


FIG. 11. P- θ diagram of oblique collision of shock waves in aluminum, $P_1 = 0.33 \times 10^{12}$ bar.

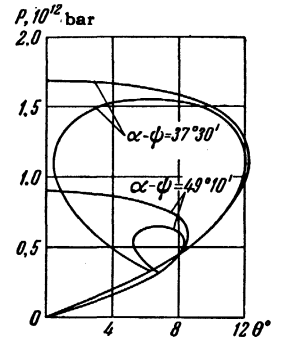


Figure 11 shows the relative positions of the polars of aluminum for the first series of experiments at $\alpha - \psi = 37^\circ 30'$ and $\alpha - \psi = 49^\circ 10'$. A similar picture occurs for copper (Fig. 12) at $\alpha - \psi = 37^\circ 30'$ and $\alpha - \psi = 44^\circ$, and also for lead and iron. For all four metals, the polars Π_2 are situated inside the polars Π_1 and do not cross the latter. The right-hand branches of the polars Π_1 and Π_2 are quite close to each other. These features are equally typical of the P- θ diagrams for

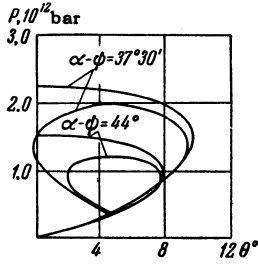


FIG. 12. P-θ diagram of oblique collision of shock waves in copper. $P_1 = 0.37 \times 10^{12}$ bar.

the collisions of "weak" shock waves in air (see Fig. 8a).

Optical registration of three-shock modes in air yields, in addition to the angles $\alpha - \psi$, also information on the reflection angle β . The values of α , ψ , and β for air are given by Bleakney and Taub^[1] for both "weak" and "strong" shock waves. Using these values, we have calculated the state parameters behind the front of the reflected wave. For "strong" shock waves, in accordance with the simplest scheme of three-shock flow, the coordinates of the reflection region are determined (Fig. 8) by the point of intersection of the polars. For weak shock waves, this scheme might be realized for states situated on the right branches of the Π_2 polars, which merge with the right branches of the Π_1 polars. Actually, however, in collisions between weak shock waves in air (Fig. 8a) the coordinates P and θ of region 2 correspond to the upper portion of the polar Π_2 , which is a considerable distance from Π_1 . The modes occurring in this case can of course not be described by a flow with a single tangential discontinuity. This deduction applies to collisions of weak waves in air equally well as to the collisions of weak waves in metals.

The condition for the existence of flow with one tangential discontinuity is thus that the polars intersect to the left of the vertical $\theta = \theta_1$. The presence or absence of these intersections depends obviously on the relative dimensions of the polars. Their relative magnitudes are determined in turn by the relative locations of the single and twofold compression adiabats on the P- ρ or P-v diagrams. The polars intersect if the adiabats of the second shock are more gently sloping and lie appreciably below the adiabat of the single compression.

Similar adiabats are observed for shock waves of large amplitude, when the thermal pressures in the shock compression begin to play an appreciable role. Calculations show that in the second series of experiments crossings of polars at a collision angle $2\alpha = 90^\circ$ occur for aluminum but still not for iron, copper, or lead. The P- θ diagram calculated from the equation of state^[9] is shown in Fig. 13. The numbers on the polar Π_1

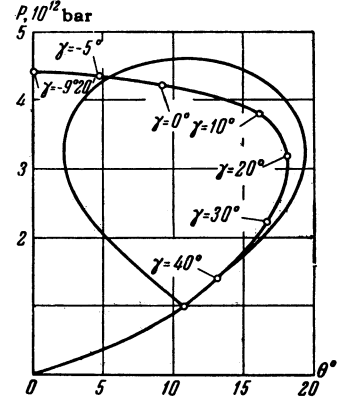


FIG. 13. P-θ diagram of oblique collision of shock waves in aluminum. $\alpha - \psi = 35^\circ 40'$; $\psi = 9^\circ 20'$; $P_1 = 0.99 \times 10^{12}$ bar.

denote the bend angles of the leading wave for different points of the polar Π_1 .

3. DETERMINATION OF THE PARAMETERS OF THE REGION OF TWOFOLD COMPRESSION BEHIND THE REFLECTED WAVE

The experimentally observed characteristics of the irregular modes can be used to study the compressibility at rather high colliding-wave pressures. For flow conditions corresponding to the model with a single tangential discontinuity, the parameters of the region of twofold compression behind the front of the reflected wave are determined from the experimental values of $\alpha - \psi$ and $\varphi = \gamma + \psi$. We must also know the parameters of the incident shock wave and the single compression adiabat at the collision pressures given by the relation $\Delta U_{30} = f(D_{30})$.

Knowing the foregoing quantities, we can successively determine the vector \mathbf{q}_0 , the direction and magnitude of the vectors \mathbf{D}_{30} and $\Delta \mathbf{U}_{30}(D_{30})$, the direction of the tangential discontinuity AT along the vector $\mathbf{q}_3 = \mathbf{q}_0 + \Delta \mathbf{U}_{30}$, and the pressure on the front of the leading wave

$$P_{30} = \rho_0 D_{30} \Delta U_{30}, \tag{6}$$

which is equal to the pressure in region 2. An independent expression for the latter is the equation

$$P_2 = P_1 + \rho_1 D_{21} \Delta U_{21} \tag{7}$$

which represents the conservation of the momentum as \mathbf{q}_1 crosses the front of the reflected wave.

The conditions that P_2 and P_3 be equal, as can be readily shown, are fulfilled for all vectors $\Delta \mathbf{U}_{21}$ that terminate on the chord MN (Fig. 7) perpendicular to the vector \mathbf{q}_1 and located at a distance

$$\Delta q_1 = (P_3 - P_1) / \rho_1 q_1 \tag{8}$$

away from its right end.

From the condition that \mathbf{q}_2 must be parallel to \mathbf{q}_3 it follows that the vector $\Delta \mathbf{U}_{21}$ also terminates

Table III

Metal	$P_1, 10^{12}$ bar	α	ψ	τ	$D_{20}(A),$ km/sec	$D_{20}(C),$ km/sec	$P_{20}(A),$ 10^{12} bar	$P_{20}(C),$ 10^{12} bar
Aluminum	0,97	45°	9°20'	0	17,36	17,36	4,25	4,25
Copper	1,79	45°	10°	14°	12,39	13,07	6,28	7,21
Lead	1,75	45°40'	8°30'	—	—	—	—	—
Iron	1,71	45°40'	8°50'	8°	13,10	13,38	6,08	6,42

on the tangential discontinuity line AT. The intersection between the chord MN and the tangential discontinuity determines the directions and magnitudes of the vectors ΔU_{21} and D_{21} , and consequently the density

$$\rho_2 = \rho_1 D_{21} / (D_{21} - \Delta U_{21})$$

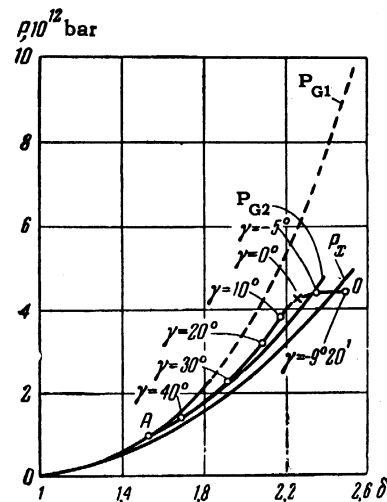
behind the front of the reflected waves, acquired by the investigated substance after successive application of the pressures P_1 and $P_2 = P_3$.

The method developed here is not universal. The possibility and usefulness of its application call for a preliminary analysis, based on the use of the approximate equations of state of the investigated substances. As follows from the data given in the preceding section, the procedure for measuring the twofold compressibility under conditions of oblique collision between strong shock waves can be used, in particular, to investigate the equation of state of aluminum. The parameters of the collision region were calculated for this metal using the above method and the data of Tables I and III.

The results of the investigation of the twofold compressibility of aluminum are shown on the P - δ (pressure vs. relative compression) diagram in Fig. 14. The diagram shows the single compression adiabat P_{G1} with its experimentally determined^[6] and extrapolated^[9] isotherm P_x for 0°K and the adiabat P_{G2} of the second shock. The line OA represents (in P - δ coordinates) the possible points of intersections of the polars for different angles γ (see Fig. 13). Modes with a single tangential discontinuity cannot be realized for twofold compression adiabats located to the left of OA (more accurately, to the left of the point on this line with $\gamma = 3^\circ$). The resultant experimental point of twofold compression of aluminum is marked by a cross in the figure. It is located somewhat above the calculated adiabat P_{G2} . The compression curve at absolute zero should be raised by approximately the same amount.

Figure 14 shows that the collision causes the pressure behind the front of the reflected wave to rise to 4.25×10^{12} bar, i.e., approximately 4 times,

FIG. 14. Curves showing the compressibility of aluminum: P_{G1} - dynamic adiabat of single compression; P_{G2} - calculated adiabat of two-fold compression, P_x - calculated isotherm at 0°K, x - experimental point of twofold compression, OA - trajectory of the points of intersection of the polars.



while the increase in density is 1.5-fold. Relative to the normal state of aluminum, its density increases 2.26 times to 6.2 g/cm³.

A study of oblique collisions of shock waves was started by the authors some 10 years ago. In the first series of researches, the most active part in the laborious and complicated experiment was played by M. P. Speranskaya, the late N. S. Tenigin, A. N. Kolesnikova, M. S. Shvetsov, and L. N. Gorelova. Some of the results on aluminum and lead were obtained by M. V. Sinitsyn. Many valuable hints were made by Ya. B. Zel'dovich and S. A. Khristianovich. The authors are deeply grateful to all these persons.

¹W. Bleakney and A. H. Taub, *Revs. Modern Phys.* **21**, 584 (1949).

²L. D. Landau and E. M. Lifshitz, *Mekhanika sploshnykh sred* (Mechanics of Continuous Media), Gostekhizdat, 1954.

³R. Courant and K. O. Friedrichs, *Supersonic Flow and Shock Waves*, Interscience, N.Y., 1948.

⁴O. S. Ryzhov and C. A. Khristianovich, *PMM* (Applied Mechanics and Mathematics) **22**, 586 (1958).

⁵E. A. Feoktistova, *DAN SSSR* **136**, 1325 (1961), *Soviet Phys.-Doklady* **6**, 162 (1961).

⁶ Al'tshuler, Kormer, Bakanova, and Trunin, JETP **38**, 790 (1960), Soviet Phys. JETP **11**, 573 (1960).

⁷ Al'tshuler, Krupnikov, Ledenev, Zhuchikhin, and Brazhnik, JETP **34**, 874 (1958), Soviet Phys. JETP **7**, 606 (1958).

⁸ V. N. Zharkov and V. A. Kalinin, DAN SSSR

135, 811 (1960), Soviet Phys. Doklady **5**, 1253 (1961).

⁹ Kormer, Urlin, and Popova, FTT **3**, 2131 (1961), Soviet Phys.-Solid State **3**, 1547 (1962).

Translated by J. G. Adashko
239